Asian Journal of Chemistry; Vol. 34, No. 1 (2022), 42-52

ASIAN JOURNAL OF CHEMISTRY

https://doi.org/10.14233/ajchem.2022.23409

Efficient Synthesis, Spectral, Characterization, Antimicrobial and DFT Studies of Antimony(III) Dithiocarbamates

S. TAMILVANAN

Department of Chemistry, Annamalai University, Annamalainagar-608002, India

Corresponding author: E-mail: laksuntam@gmail.com

Received: 11 July 2021; *Accepted*: 30 August 2021; *Published online*: 16 December 2021; AJC-20617

The synthesis and characterization of novel antimony(III) dithiocarbamate complexes *tris*(*N*-furfuryl-*N*-propyldithiocarbamato-S,S′)antimony(III) (**1**) and *tris*(*N*-furfuryl-*N*-butyldithiocarbamato-S,S′)antimony(III) (**2**) have been characterized by elemental analysis, FT-IR, NMR (^{1}H and ^{13}C) spectra and antimicrobial studies. The characteristic thioureide ($\nu_{C\text{-}N}$) bands occur at 1462 and 1475 cm^{-1} for complex **1** and **2**, respectively. The theoretical calculations of the complexes have been carried out by density functional theory (DFT). The FMOs, MEP, Mulliken charge distribution and chemical activity parameters of the optimized structure have been calculated at the same level of theory. The MEP structure indicated that the positive and negative potential sites are around hydrogen atoms and electronegative atoms of the studied complexes, respectively. The Agar-well diffusion method were used to study the antimicrobial activity of the complexes against two Gram-positive bacteria (*Klebsiella pneumoniae* and *Staphylococcus aureus*), two Gram-negative bacteria (*Escherichia coli* and *Vibrio cholera*) and two fungal organisms (*Candida albicans* and *Aspergillus niger*).

Keywords: Antimony, Dithiocarbamate, DFT, Microorganism.

INTRODUCTION

The persistent interest in the dithiocarbamate complex of antimony could be attributed to many reasons. These consist of their structural diversity, which range from monomeric to polymeric supramolecular assemblies and their unique application as biological catalysts and utilization in surface chemistry [1-3]. Metal dithiocarbamates are the amides of dithiocarbamic acid and are proficient of forming stable metal complexes due to their excellent coordination properties [4]. Dithiocarbamates have a wide range of applications and chemistry, thus resulting in their adaptability. Insoluble nature of dithiocarbamate and its derivatives, they have been widely used in inorganic analysis and also for the separation of metal ions in HPLC and GC. Dithiocarbamates have found usage as fungicides, pesticides, production of petroleum derivatives, lubricants, polymers and they are used as accelerators (ZDMC, ZDBC, ZDEC, ZBEC) in rubber vulcanization, antioxidants and antihumidity [5]. Dithiocarbamates are used as secondary accelerators to activate the primary accelerators. The readily obtainable strong binding site of the two sulfur atoms within their structure of complex confer a large ionic radius; consequently, dithiocarbamates have exposed the ability to bind strongly in 9 different modes to a metal atoms [6,7]. This functional group (CSS) of the dithiocarbamate derivative is often obtaining through a CS_2 insertion reaction with either a primary amine or secondary amine complex [7]. A resonance between two sulfur atoms consequently allows different binding modes with a variety of metal ions. Synthesis and the reactivity of transition metal dithiocarbamate complexes, with various structural geometry have been carried out [8].

Medicinal use of antimony complexes dates back to the 16th and 17th centuries, *e.g.* antimony(III) potassium tartrate (tartar emetic) was used to cure a lot of diseases, like typhoid, lung diseases (pneumonia), snail fevers, *etc.* [9]. Recently, three antimonials are under clinical use, *i.e.* pentostam (sodium stibogluconate), stibophen and glucantime (meglumine antimoniate), the latter being recommended by WHO as the first choice drug against all types of leishmaniasis [10-15]. However, many antimony complexes have been synthesized with very capable biological potential *i.e.* antimony aminocarboxylic acids showed outstanding antineoplastic activity, while some related comp-

lexes featured high biological potential and have been applied medically [16]. As far as dithiocarbamate compounds are concerned, two dimethyl substituted polymorphs, $[SbCl(S_2CNMe_2)_2]_n$, were incredibly active against MCF-7 cancer cell lines, with IC_{50} values [17,18]. Remarkably, this activity was greater than the Food and Drug Administration (FDA) approved drugs doxorubicin and cisplatin [19,20]. Their results showed 158-340 (MCF-7 cell line) and 21-53 (HeLa cell line) times greater cytotoxicity than cisplatin against MCF-7 and HeLa cell lines, respectively [21]. This statistics clearly indicates the great potential of antimony complexes and hence demands their further investigation in the biological domain.

Metal dithiocarbamate complexes and their diverse applications in organic synthesis, medicine, agriculture and precursors for metal sulphide and metal oxide nanoparticles [22]. Antimony complexes have been reported to prove great feasible as medicinal agents. A variety of crystal structures of antimony(III) dithiocarbamates have been studied [23] owing to their diverse applications either related to biological or chemical endeavors. Many of such compounds exhibit peculiar and infrequently surprising features [24]. In extension of our new interest in main group metal compounds of sulfur donor ligands, we report herein the efficient synthesis, spectral, characterization, antimicrobial and DFT studies of antimony(III) dithiocarbamates. In the present study, IR and NMR spectral investigations of the complexes **1**-**2** have been performed using DFT. Geometry optimization calculations were performed for the B3LYP theory measure with LANL2DZ basis set. In addition, HOMO-LUMO, Mulliken charge analysis and MEP analysis of information have been used to support the structural properties. The successfully introduced two new synthetic complexes, *tris*(*N*-furfuryl-*N*-propyldithiocarbamato-S,S′)antimony(III) (**1**), *tris*(*N*-furfuryl-*N*-butyldithiocarbamato-S,S′)antimony(III) (**2**) characterized by IR, CHN analysis, ^1H & ^{13}C NMR and antimicrobial activity. In addition, density functional theory (DFT) investigations were performed on synthesized new antimony(III) dithiocarbamates in order to validate the experimental work.

EXPERIMENTAL

All the chemicals, solvents and reagents were analytical grade and used without further purification. Melting points were determined for the complexes by thermal melting point apparatus and used with open capillary tubes. Elemental analysis (carbon, hydrogen & nitrogen) was performed at sophisticated analytical instrument facility Centre, CDRI, Lucknow, India (elementar analyse systeme Gmbh Vario El V3.00) and the Emcure Pharmaceuticals Ltd, Api Research Centre, Pune (vario MICRO V2.2.O). FT-IR spectra were taken suitably as KBr discs of the compound. The complex were ground to fine powder and mixed with KBr and then ground again to mix thoroughly. The KBr sample mixture was then pressed into a thin disc. FT-IR spectra of the synthesized complexes were recorded in the region 4000-400 cm^{-1} using Thermo SHIMADZU FT-IR spectrophotometer. ^1H & ^{13}C NMR spectra were recorded on a BRUKER 400 MHz spectrometer model using $CDCl_3$ as a solvent for all the complexes. The Bruker spectrometer operates at 400 MHz for ^1H spectra and 100 MHz for ^{13}C NMR spectra. Chemical shifts are reported in ppm relative to standard. Tetramethylsilane was used as an internal reference for ^1H and ^{13}C NMR spectra.

Synthesis of antimony(III) dithiocarbamate complexes (1-2): Furfuraldehyde was added to primary amine (propylamine, butylamine) in methanol and the mixture was allowed stir for 2 h. The solvent was removed by evaporation. The resultant oily product was dissolved in methanol-dichloromethane solvent mixture. To this solution excess sodium borohydride was added slowly at 5 ºC and stirred for 2 h before removal of ice bath. The reaction mixture was allowed stir for 12 h at room temperature. After evaporation of the solvent, the resulting viscous liquid was washed with water and dichloromethane was added in order to extract the product. Evaporation of the organic layer yielded furfuryl based secondary amine [25].

***tris*(*N*-Furfuryl-*N*-propyldithiocarbamato-S,S′)-antimony(III) (1):** Furfuryl based secondary amine and carbon disulfide were dissolved in ethanol and the reaction mixture was stirred for 0.5 h under ice cold condition. Antimony trichloride was added to the solution. The yellowish solids were obtained by filtration and washed with water and dried. The obtained product was recrystallized to get the outstanding yield (**Scheme-I**). Yield: 83%, m.p.: 163 ºC. Anal. calcd. (found) % for $C_{27}H_{36}N_3O_3S_6Sb$ (*m.w.* 764.74): C, 42.40 (42.35); H, 4.74 (4.70); N, 5.49 (5.45). IR (KBr, cm^{-1}): Experimental: 1462 ν(C-N), 1015 ν(C-S), 2848 ν(C-H), Theoretical: 1468 ν(C-N), 1041 ν(C-S), 2964 ν(C-H), ^1H NMR (400 MHz, $CDCl_3$, ppm): Experimental: 0.89 (t, 9H, *J* = 7.5 Hz, N–CH_2–CH_2–$C\underline{H}_3$); 1.68 (m, 6H, *J* = 8.0 Hz, N–CH_2–$C\underline{H}_2$–CH_3); 3.69 (t, 6H, *J* = 8.0 Hz, N–$C\underline{H}_2$–CH_2–CH_3); 5.01 (s, 6H, CH_2 furfuryl); 6.39 (d, 3H, H–3 (furyl); 6.23 (dd, 3H, H–4 (furyl); 7.01 (d, 3H, H–5 (furyl): Theoretical: 0.166 (H18, H19, H66) (N–CH_2–CH_2–$C\underline{H}_3$); 0.9678 (H15, H16) (N–CH_2–$C\underline{H}_2$–CH_3); 2.8450 (H13, H67) (N–$C\underline{H}_2$–CH_2–CH_3); 3.7987 (H21, H68) (CH_2 furfuryl); 5.9701 (H75) (furyl); 6.3601 (H73) (furyl); 7.0742 (H76) (furyl). ^{13}C NMR (100 MHz, $CDCl_3$, ppm) Experimental: 11.9 (CH_2-CH_2-$\underline{C}H_3$); 20.8 (CH_2-$\underline{C}H_2$-CH_3); 49.2 ($\underline{C}H_2$-CH_2-CH_3); 56.6 (CH_2 furfuryl); 110.9, 142.6, 148.2 (furyl ring carbons); 202.8 (NCS_2): Theoretical: 4.0743 (C17) (CH_2-CH_2-$\underline{C}H_3$); 13.3490 (C14) (CH_2-$\underline{C}H_2$-CH_3); 50.8244 (C12) ($\underline{C}H_2$-CH_2-CH_3); 43.82420 (C20) (CH_2 furfuryl); 104.8690 (C72), 105.58057 (C70), 139.5719 (C74), 152.22056 (C69) (furyl ring carbons); 226.2653 (C11) (NCS_2).

***tris*(*N*-furfuryl-*N*-butyldithiocarbamato-S,S′)-antimony(III) (2):** A similar procedure as described in complex **1** was employed for the preparation of complex **2**. Yield: 79%, m.p.: 155 ºC. Anal. calcd. (found) % for $C_{30}H_{42}O_3N_3S_6Sb$ (*m.w.* 806.82): C, 44.66 (44.60); H, 5.25 (5.21); N, 5.21 (5.19). IR (KBr, cm^{-1}) Experimental: 1475 ν(C-N), 1010 ν(C-S), 2910 ν(C-H). Theoretical: 1463 ν(C-N), 1031 ν(C-S), 2952 ν(C-H). ^1H NMR (400 MHz, $CDCl_3$, ppm) Experimental: 0.97 (t, 9H, *J* = 7.5 Hz, N–CH_2–CH_2–CH_2–$C\underline{H}_3$); 1.26 (m, 6H, N–CH_2–CH_2–$C\underline{H}_2$–CH_3); 1.69 (m, 6H, *J* = 2.0 Hz; N–CH_2–$C\underline{H}_2$–CH_2–CH_3); 3.67 (t, 6H, *J* = 8.0 Hz; N–$C\underline{H}_2$–CH_2–CH_2–CH_3); 5.14 (s, 6H, CH_2 furfuryl); 6.52 (d, 3H, H–3 (furyl); 6.43 (dd, 3H, H–4 (furyl); 7.32 (d, 3H, H–5 (furyl): Theoretical: 0.1635

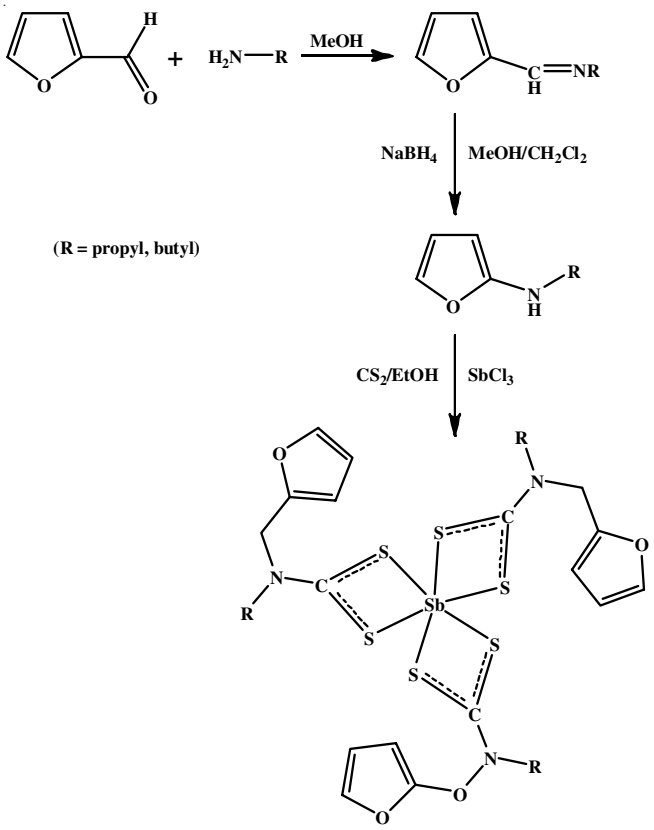

Scheme-I: Schematic presentation for the synthesis of the antimony complexes

(H83, H84, H85) (N–CH_2–CH_2–CH_2–C$\underline{H}_3$); 0.4805 (H18, H63) N–CH_2–CH_2–C$\underline{H}_2$–CH_3); (0.9187 (H15, H16) N–CH_2–C$\underline{H}_2$–CH_2–CH_3); 2.8255 (H13, H64) N–C$\underline{H}_2$–CH_2–CH_2–CH_3); 3.7921 (20H, 65H) (CH_2 furfuryl); 5.9081 (H72) (furyl); 6.3586 (H70) (furyl); 7.0707 (H73) (furyl): ^{13}C NMR (100 MHz, $CDCl_3$, ppm) Experimental: 13.1 (CH_2-CH_2-CH_2-C$\underline{H}_3$); 20.9 (CH_2-CH_2-C$\underline{H}_2$-CH_3), 27.8 (CH_2-C$\underline{H}_2$-CH_2-CH_3); 49.9 (C$\underline{H}_2$-CH_2-CH_2-CH_3); 52.8 (CH_2 furfuryl); 110.9, 142.1, 148.5 (furyl ring carbons); 203.1 (NCS_2): Theoretical: 7.5735 (C82) (CH_2-CH_2-CH_2-C$\underline{H}_3$); 15.3418 (C17) (CH_2-CH_2-C$\underline{H}_2$-CH_3), 22.9092 (C14) (CH_2-C$\underline{H}_2$-CH_2-CH_3); 49.9816 (C12) (C$\underline{H}_2$-CH_2-CH_2-CH_3); 43.8672 (C19) (CH_2 furfuryl); 104.7079 (C69), 105.4862 (C67) 139.5458 (C71) 152.1351 (C66) (furyl ring carbons); 226.1335 (C11) (NCS_2).

Computational studies: The molecular geometry optimization of antimony(III) complexes were performed by employing the density functional theory (DFT) at B3LYP (Becke 3-parameter exchange functional together with the Lee-Yang-Parr correlation functional) level and LANL2DZ basis set with the help of Gaussian 09W program package [26]. However, the most optimized structural parameters such as bond length, bond angle and dihedral angle were obtained from Gaussian 09W software. The vibrational frequencies and geometry optimization for the complexes were calculated. The ^{1}H & ^{13}C NMR spectra were calculated using the GIAO method using chloroform solvent with TMS reference. The optimized structures of the complexes have been used to calculate the highest occupied molecular orbital and lowest unoccupied molecular orbital [27] images were visualized using Gauss View 5. Electrophilicity, Mulliken charge distribution of atoms [28] of systems were calculated. The nucleophilic and electrophilic regions were identified by molecular electrostatic potential (MEP) [29] was visualized using Gauss View 5. Moreover, many other parameters like total energy, molecular dipole moment for the present complexes have been also presented. All the complexes were performed on a personal computer by using the Gaussian 09W software package.

Antimicrobial studies: The cultures of microorganism (*Escherichia coli*, *Staphylococcus aureus*, *Klebsiella pneumoniae*, *Vibrio cholera*e, *Candida albicans* and *Aspergillus niger*) were incubated test plates by Mueller Hinton Agar-well diffusion technique [30]. The cultures of the test microorganism were prepared in sterile nutrient broth medium and incubated for 24 h at 37 ºC for the bacteria and 27 ºC for fungal. The sterile antibiotic disc (6 mm diameter) loaded with different concentrations (400 and 800 µg/mL) of antimony(III) complexes **1** and **2** were placed on the spread plates. The spread plates were incubated for 24 h. Afterwards, the zones of inhibition were examined and recorded in millimeter as the activity against the tested pathogens. Ciprofloxacin was used as the reference drug.

RESULTS AND DISCUSSION

FT-IR analysis: The FT-IR spectra of the complexes gave bands between 4000 and 400 cm^{-1} from which information about the coordination mode (monodentate/bidentate) of the dithiocarbamate ligands to the metal ions. The $\nu_{C\text{-}N}$ (thioureide) stretching bands of the dithiocarbamate complexes occurred as sharp bands in the range 1550-1450 cm^{-1}. The ($\nu_{C\text{-}S}$) stretching vibration is appeared as single bands in the region of 1050-950 cm^{-1} in all the Sb(III) complexes and indicates a symmetrical bonding of the sulfur atoms of the ligand to the central metal ion [31]. For complexes **1** and **2,** the thioureide ν(C-N) bands are observed at 1462 and 1475 cm^{-1}, which where theoretically calculated as 1468 and 1463, respectively. The ν(C-S) stretching vibrations bands are around 1015, 1010 cm^{-1} in complexes **1**, **2** respectively, where theoretical calculation bands at 1041 and 1031 cm^{-1} using B3LYP computation method. The ($\nu_{C\text{-}S}$) symmetry stretching vibrations supporting the bidentate mode of the ligand to metal center. The aromatic $\nu_{C\text{-}H}$ bands are observed in the range 2910-2848 cm^{-1}. This band is characteristic of NCS_2 band with an intermediate bond between single bond (1350-1250 cm^{-1}) and double bond (1690-1640 cm^{-1}) [32]. The ν(M-S) stretching bands for metal dithiocarbamate complexes usually fall below 400 cm^{-1} and that could not be observed due to the FT-IR spectral range of the measurements. FT-IR spectra of complexes 1 and 2 are given in Fig. 1.

NMR analysis: ^{1}H and ^{13}C NMR spectra of complexes **1** and **2** are given in Fig. 2. ^{1}H NMR spectra were characteristic of each dithiocarbamate ligand type. Thus complex **1** showed three signals (0.89, 1.68 and 3.69 ppm) associated with the CH_2 and CH_3 group of propyl that bound to nitrogen appear at relatively lowfield, which were found the signals (0.16, 0.96 and 2.84 ppm) based on the theoretical spectrum. The sharp intense signal at 5.01 ppm assigned to the CH_2 of furfuryl. The aromatic protons observed in the downfield region in the

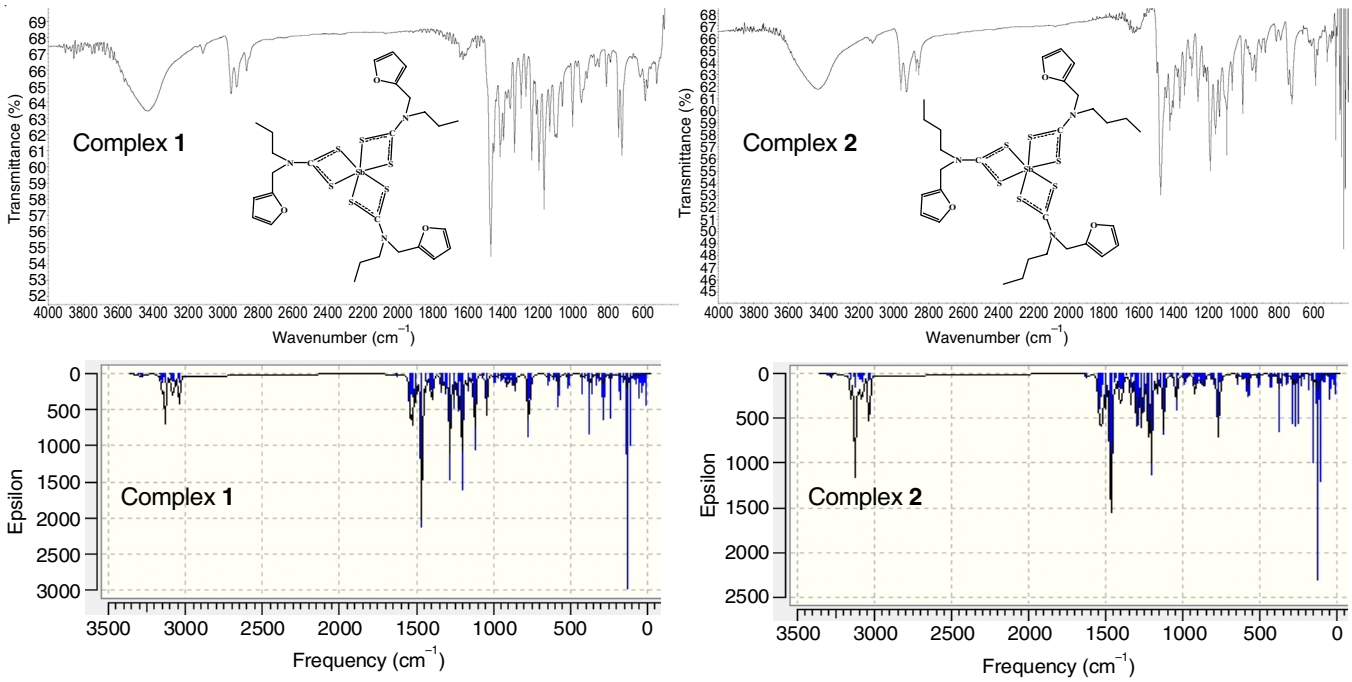

Fig. 1. Experimental (up) and theoretical (down) infrared spectra of complexes **1** and **2**

range 6.39-7.01 ppm, which were theoretically observed in the range 6.36-7.07 ppm. For complex **2**, signals observed at 5.14 and 3.67 ppm are due to CH_2 protons of furfuryl and N-CH_2 (butyl) protons, respectively. The remaining signals in the aliphatic region are assigned to the other CH_2 protons and CH_3 protons of butyl groups. Two signals observed in the aliphatic region are due to the CH_2 protons of furfuryl and aromatic, which were theoretically calculated. In all the complexes, CH_2 protons neighbouring to nitrogen atom are deshielded to a great extent on complexation compared to the free amines.

The NCS_2 1,1-thiolate carbon signals are observed in the expected region (around δ 200 ppm) for main group dithiocarbamate complexes [33]. In complexes **1** and **2**, these signals are observed around δ 202.9 ppm, representing contribution of double bond character to a formally single N–C bond in the dithiocarbamate ligand, which were theoretically observed around δ 226.2 ppm using the GIAO (gauge-invariant atomic orbital) method [34]. For complexes **1** and **2**, the signals for CH_2 carbons adjacent to nitrogen atoms are observed in the region 49.2-56.6 ppm. The other two and three signals observed in the aliphatic region for complexes **1** and **2**, respectively are assigned to the other carbons of propyl and butyl groups.

Geometry of the molecule: The optimized molecular structure of the Sb(III) complexes **1** and **2** are given in Fig. 3. The calculated bond distance, bond angle and dihedral angle for the main group dithiocarbamate complexes **1** and **2**. The C-N (thioureide) and C-S bond distances in the structure of complex **1** lies between 1.351-1.353 Å and 1.770-1.815 Å, respectively. The bond angle and dihedral angle of the complex **1** found to be 64.7º (S2-Sb1-S3) and -176.5º (S6-C33-N10-C36), respectively. The structural parameters of complexes **1** and **2** are listed in Tables 1 and 2.

Frontier molecular orbitals (FMOs): The highest occupied molecular orbital (HOMO) and lowest unoccupied molecular

TABLE-1
OPTIMIZED GEOMETRIC PARAMETERS OF COMPLEX **1**

Bond distances (Å)		Bond angles (°)		Dihedral angles (°)	
S2-Sb1	3.050	S2- Sb1-S3	64.7	S6-C33-N10-C36	-176.5
S3- Sb1	2.713	S4- Sb1-S5	64.6	S7-C33-N10-C34	-177.1
S4- Sb1	3.054	S6- Sb1-S7	64.6	N10-C36-C38-C41	-178.2
S5- Sb1	2.712	S3- C11-S2	119.4	N10-C34-C45-C46	88.0
S6- Sb1	3.053	S3- C11-N8	118.0	H53-C36-C38-H39	-177.9
S7- Sb1	2.714	S2- C11-N8	122.4	S2-C11-N8-C12	178.4
C11-S2	1.770	C12-N8- C20	115.1	S3-C11-N8-C20	179.01
C11-S3	1.817	S4- C22-S5	119.4	N8-C20-C69-C70	-91.2
C11-N8	1.352	S4- C22-N9	122.5	N8-C12-C14-C17	178.1
C22-S4	1.770	S5- C22-N9	118.0	H67-C12-C14-H15	178.2
C22-S5	1.817	C25-N9- C23	115.1	S5-C22-N9-C23	178.5
C22-N9	1.351	S6- C33-S7	119.3	S4-C22-N9-C25	178.2
C33-S6	1.771	S6- C33-N10	122.5	N9-C23-C58-C59	-92.0
C33-S7	1.815	S7- C33-N10	118.1	N9-C25-C30-C27	178.6
C33-N10	1.353	C36-N10- C34	116.3	H56-C25-C30-H31	178.6

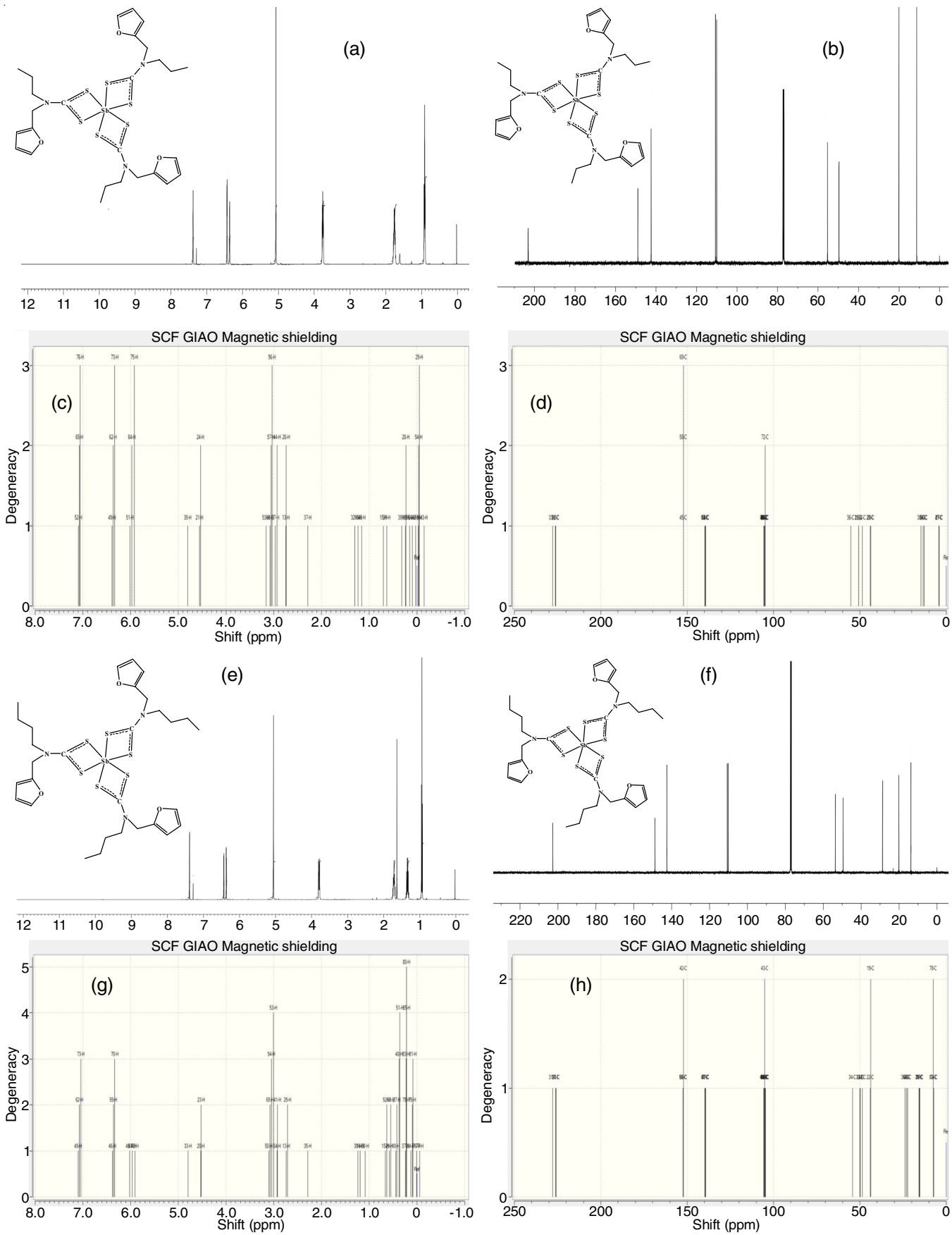

Fig. 2. Experimental (up) and theoretical (down) NMR spectra of complexes **1** and **2**; [(a,c) - ^{1}H and (b,d) ^{13}C NMR for **1**] [(e,g) - ^{1}H and (f,h) ^{13}C NMR for **2**]

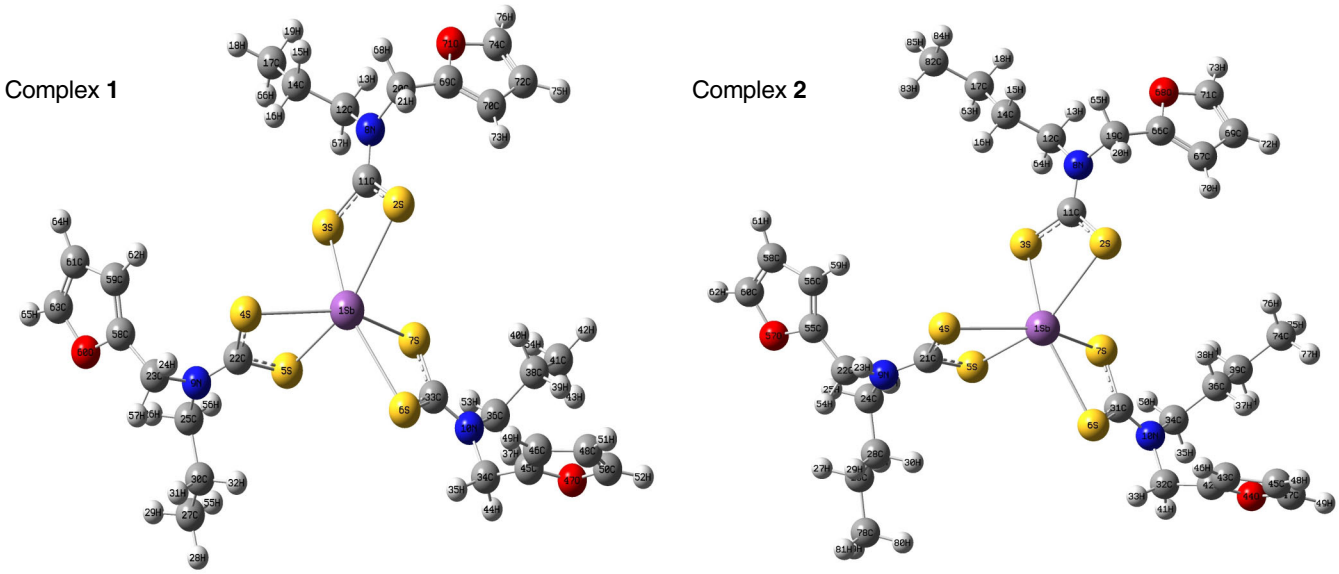

Fig. 3. Optimized geometric structure of antimony(III) complexes **1** and **2**

TABLE-2
OPTIMIZED GEOMETRIC PARAMETERS OF COMPLEX **2**

Bond distances (Å)		Bond angles (°)		Dihedral angles (°)	
S2-Sb1	3.051	S2- Sb1-S3	64.7	S6-C31-N10-C34	-176.4
S3- Sb1	2.713	S4- Sb1-S5	64.6	S7-C31-N10-C32	-177.1
S4- Sb1	3.053	S6- Sb1-S7	64.6	N10-C32-C42-C43	88.1
S5- Sb1	2.712	S3- C11-S2	119.4	N10-C34-C36-C39	-177.7
S6- Sb1	3.052	S3- C11-N8	118.0	H38-C36-C39-H40	-179.0
S7- Sb1	2.714	S2- C11-N8	122.4	S2-C11-N8-C12	178.2
C11-S2	1.770	C12-N8- C19	115.0	S3-C11-N8-C19	178.7
C11-S3	1.817	S4- C21-S5	119.4	N8-C12-C14-C17	178.7
C11-N8	1.351	S4- C21-N9	122.5	N8-C19-C66-C67	-92.0
C21-S4	1.770	S5- C21-N9	118.0	H84-C82-C17-H63	-178.2
C21-S5	1.817	C24-N9- C22	115.1	S5-C21-N9-C22	178.2
C21-N9	1.351	S6- C31-S7	119.3	S4-C21-N9-C24	178.2
C31-S6	1.771	S6- C31-N10	122.6	N9-C22-C55-C56	-92.1
C31-S7	1.815	S7- C31-N10	118.0	N9-C-24-C28-C26	179.3
C31-N10	1.353	C32-N10- C34	116.2	H25-C24-C28-H30	-178.9

orbital (LUMO) are name as frontier molecular orbitals (FMOs), values can provide the information about electronic, luminescence, UV-vis, photochemical reaction, pharmaceutical studies, quantum chemistry and optical properties of the materials. The FMOs energy gap supports to specify the stability of structure. It also informs about the chemical reactivity and kinetic stability of a molecule. The calculated energy gap values 4.0852 eV and 4.0789 eV for complexes **1** and **2**, respectively. The energy difference between the highest occupied molecular orbital and the lowest unoccupied molecular orbital can be used to determine the polarisability, chemical hardness, reactivity and softness values for a molecule. The highest occupied molecular orbital represents the capability to donate an electron, whereas lowest unoccupied molecular orbital, as an electron acceptor. A molecule that possesses a large energy gap is hard, less polarizable and less reactive, whereas a molecule with a small energy gap would be considered to be soft, more polarizable and more reactive [35].

Highest occupied molecular orbital (HOMO) and lowest unoccupied molecular orbital (LUMO) are very useful energy values parameters for determining global chemical reactivity such as global hard-ness (η), electrophilicity (ω), chemical potential (μ), electro-negativity (χ) and global softness (S), which have been effectively utilized to expect global chemical reactivity trends. These variables can be calculated from ionization potential (IP) and electron affinity (EA) values displayed in Fig. 4 and Table-3.

Ionization potential and electron affinity are related to the HOMO [ionization potential (IP) = $-E_{HOMO}$] and LUMO [electron affinity (EA) = $-E_{LUMO}$] energies, respectively, which are defined by Koopman's theorem [36]. Fig. 4 and Table-3 reveal that complex **1** has the highest ionization potential (IP) 5.6297 and electron affinity (EA) 1.5445 value, whereas complex **2** has the lowest ionization potential (IP) 5.6183 and electron affinity (EA) 1.5393 value. These results concur with the definitions of both properties of the complexes, as they symbolize the negative values of E_{HOMO} and E_{LUMO}. The global hardness (η) and global softness (S) variables are defined as [$\eta = ½ (E_{LUMO} - E_{HOMO}) = 2.0426$ eV] and ($S = 1/2\eta = 0.2448$ eV),

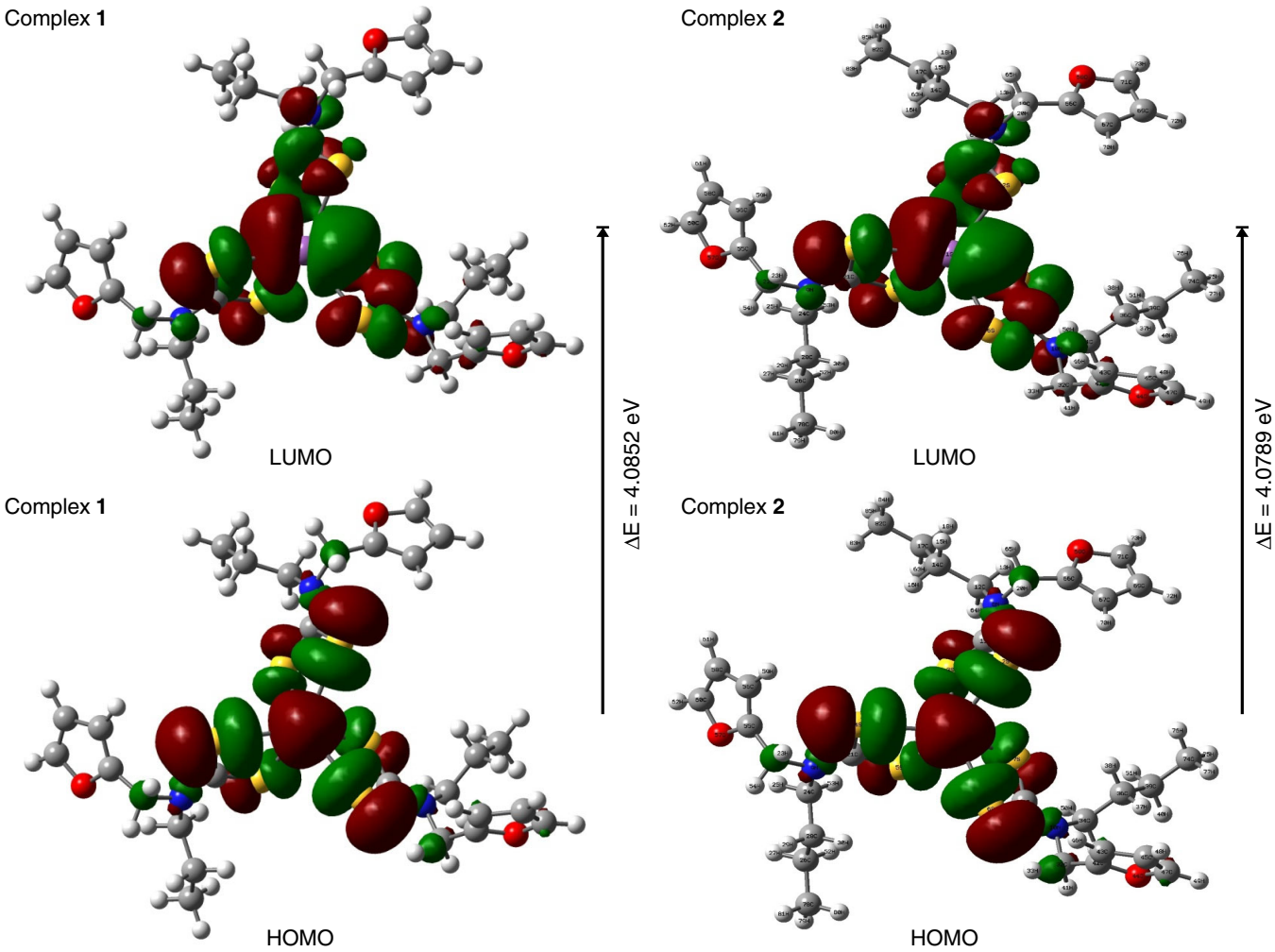

Fig. 4. HOMO-LUMO structure with the energy level plots of antimony(III) complexes **1** and **2**

TABLE-3
CALCULATED ENERGY VALUES OF COMPLEXES **1** AND **2**

Parameters	Complex **1** (eV)	Complex **2** (eV)
HOMO	-5.6297	-5.6183
LUMO	-1.5445	-1.5393
Energy Gap	4.0852	4.0789
Ionization potential (IP)	5.6297	5.6183
Electron affinity (EA)	1.5445	1.5393
Global hardness (η)	2.0426	2.0395
Chemical potential (μ)	-3.5871	-3.5788
Electronegativity (χ)	3.5871	3.5788
Global softness (S)	0.2448	0.2452
Electrophilicity index (ω)	3.1497	3.1400
Energy	-1506.2659	-1624.1863
Dipole moment (Debye)	2.7406	2.8490

respectively for complex **1**. According to the results reveal that complex **1** can be considered to be the hardest, least polarizable and least reactive. Conversely, complex **2** can be considered to be the softest, most polarizable and most reactive.

Mulliken [37] defined the electronegativity (χ) as [$\chi = -½(E_{HOMO} + E_{LUMO})$] and this global chemical reactivity represents the attraction of electrons by the activities of functional group and an atom, resulting the electronic charges from poor to richer electronegativity (χ) regions within a molecule. As shown in Fig. 4 and Table-3, complex **1** has slightly higher χ value, whereas complex **2** has the lowest χ value. The chemical potential (μ) is calculated as [$\mu = ½ (E_{HOMO} + E_{LUMO})$], which is the opposite of chemical potential (μ). As shown in Fig. 4 and Table-3, the μ value is the lower for the complex **1** and slightly higher for complex **2**.

The calculated electrophilicity (ω) values ($\omega = \mu^2/2\eta$ eV), which was defined by Parr *et al.* [38]. The electrophilicity value represents reduction in energy caused by maximal electron flow between an acceptor and a donor. Fig. 4 and Table-3 reveal that the electrophilicity value for complex **1** is the slightly higher, whereas complex **2** is the lower. Electrophilicity is considered to be good if the chemical potential value is high and global hardness is low [39].

Molecular electrostatic potential (MEP): Molecular electrostatic potential (MEP) is a valuable parameter for identifying regions where nucleophilic and electrophilic reactions may take place and is associated with electronic density and their interactions of molecule [40]. The molecular electrostatic potential surface analysis of the complexes was determined by the DFT calculation using the optimized structures with B3LYP theory measure with LANL2DZ base set. To distinguish

between regions with maximum positive potential, maximum negative potential and the potential regions between them, a colour system was implemented. The red colour in the molecular electrostatic potential surface indicates an electron-rich site, which is a negative electrostatic potential region showing electrophilic reactivity. The blue colour in the molecular electrostatic potential surface indicates an electron-deficient site, which is a positive electrostatic potential region showing nucleophilic reactivity. The regions between positive and negative potentials are represented by different colours, including green, yellow and orange. Molecular electrostatic potential increases in the order of red < orange < yellow < green < blue. Green colour in the molecular electrostatic potential surface indicates the neutral, zero electrostatic potential region showing H-bonding interactions. The colour code of the complexes lies in the range of -9.161 e^{-3} to +9.161 e^{-3} and of -9.155 e^{-3} to +9.155 e^{-3} for Sb(III) complexes **1** and **2**, respectively. The reactive sites for nucleophilic and electrophilic attack for complexes **1** and **2** are shown in Fig. 5. With molecular electrostatic potential analysis, the reactive sites can be situated by different colour codes. The polarization effect is clearly seen in the complexes. In the molecular electrostatic potential, the negative electrostatic potential regions are localized over the electronegative atoms and the positive electrostatic potential regions are localized over the hydrogen atoms. But sulfur atom of the complex is less negative potential site than the other electronegative atoms (oxygen and nitrogen). Therefore the more positive electrostatic potential and more negative electrostatic potential sites are more favourable for the attraction of electrophilic and nucleophilic species. The contour maps are a two dimensional display of the regions where the values of the virtual electron density lie within a specific range. The contour images are used to show lines of constant brightness, such as molecular electrostatic potentials and are drawn in the molecular

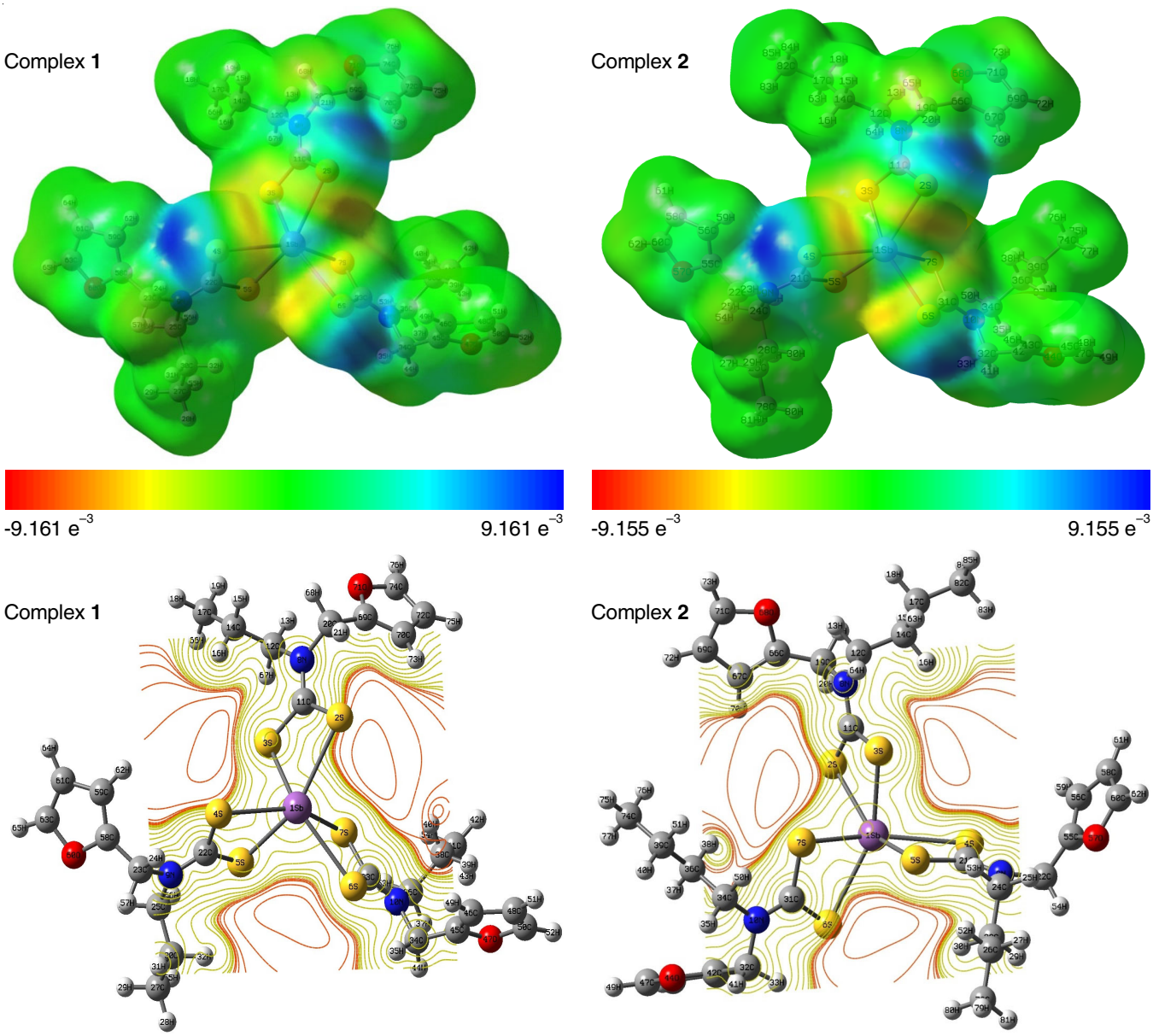

Fig. 5. Molecular electrostatic potential surface and contour of complexes **1** and **2**

plane. The electron rich lines (red) are around oxygen and nitrogen whereas electron deficient lines are shown by greenish-yellow lines. The contour map surface (Fig. 5) have been calculated by same LANL2DZ basis sets at 0.004 density with same level of calculations of the molecular electrostatic potential mapped surface of the complex.

Mulliken charge distribution: The natural population analysis of the complexes are obtained by Mulliken, which is describes the distribution of charges in the variety of sub-shells (valance, core, Rydberg) in the molecular orbital. Mulliken atomic charges of complexes **1-2** were calculated using the B3LYP theory measure with LANL2DZ basis set. The accumulation of charges on individual atom of the complexes is given in Tables 4 and 5. Mulliken atomic charge calculation plays an important role for the application of quantum chemical calculation of the molecular structure. Atomic charge affects polarizability, electronic structure, dipole moment and other molecular properties of the system. The Mulliken atomic charges on carbon (C) atoms were exhibited either negative or positive value. All hydrogen(H) atoms were displayed a net positive charge in both complexes, but H49 and H46 = 0.278 for complexes **1** and **2**, respectively were gained maximum positive charge than other hydrogen atoms in both complexes due to the presence of electronegative atoms. Some carbon atoms have a maximum positive charge of C58 (0.411), C42 (0.412). Mulliken atomic charge analysis of complexes **1** and **2** are shown in Fig. 6.

TABLE-4
MULLIKEN ATOMIC CHARGE OF COMPLEX **1**

Atom	Charge	Atom	Charge	Atom	Charge	Atom	Charge
Sb1	0.943	C20	-0.488	H39	0.207	C58	0.406
S2	-0.128	H21	0.272	H40	0.220	C59	-0.376
S3	-0.137	C22	-0.429	C41	-0.643	O60	-0.291
S4	-0.129	C23	-0.488	H42	0.206	C61	-0.246
S5	-0.140	H24	0.272	H43	0.193	H62	0.277
S6	-0.129	C25	-0.320	H44	0.228	C63	-0.154
S7	-0.134	H26	0.229	C45	0.411	H64	0.250
N8	0.027	C27	-0.638	C46	-0.376	H65	0.255
N9	0.027	H28	0.208	O47	-0.293	H66	0.206
N10	0.031	H29	0.194	C48	-0.247	H67	0.240
C11	-0.430	C30	-0.291	H49	0.278	H68	0.226
C12	-0.319	H31	0.175	C50	-0.158	C69	0.405
H13	0.229	H32	0.222	H51	0.251	C70	-0.375
C14	-0.292	C33	-0.432	H52	0.256	O71	-0.291
H15	0.175	C34	-0.492	H53	0.233	C72	-0.246
H16	0.221	H35	0.269	H54	0.203	H73	0.277
C17	-0.638	C36	-0.305	H55	0.205	C74	-0.155
H18	0.207	H37	0.201	H56	0.239	H75	0.250
H19	0.194	C38	-0.294	H57	0.226	H76	0.255

TABLE-5
MULLIKEN ATOMIC CHARGE OF COMPLEX **2**

Atom	Charge	Atom	Charge	Atom	Charge	Atom	Charge
Sb1	0.944	C22	-0.487	C43	-0.377	H64	0.244
S2	-0.129	H23	0.272	O44	-0.293	H65	0.226
S3	-0.137	C24	-0.360	C45	-0.247	C66	0.406
S4	-0.129	H25	0.232	H46	0.278	C67	-0.376
S5	-0.140	C26	-0.297	C47	-0.158	O68	-0.291
S6	-0.130	H27	0.175	H48	0.251	C69	-0.247
S7	-0.134	C28	-0.286	H49	0.256	H70	0.277
N8	0.035	H29	0.1674	H50	0.236	C71	-0.155
N9	0.035	H30	0.216	H51	0.183	H72	0.250
N10	0.037	C31	-0.437	H52	0.186	H73	0.255
C11	-0.436	C32	-0.491	H53	0.244	C74	-0.656
C12	-0.360	H33	0.269	H54	0.227	H75	0.199
H13	0.231	C34	-0.347	C55	0.406	H76	0.202
C14	-0.286	H35	0.204	C56	-0.377	H77	0.196
H15	0.167	C36	-0.284	O57	-0.291	C78	-0.653
H16	0.215	H37	0.197	C58	-0.247	H79	0.201
C17	-0.297	H38	0.214	H59	0.277	H80	0.202
H18	0.175	C39	-0.299	C60	-0.155	H81	0.195
C19	-0.488	H40	0.174	H61	0.250	C82	-0.653
H20	0.272	H41	0.228	H62	0.255	H83	0.202
C21	-0.435	C42	0.412	H63	0.187	H84	0.194
H85	0.202						

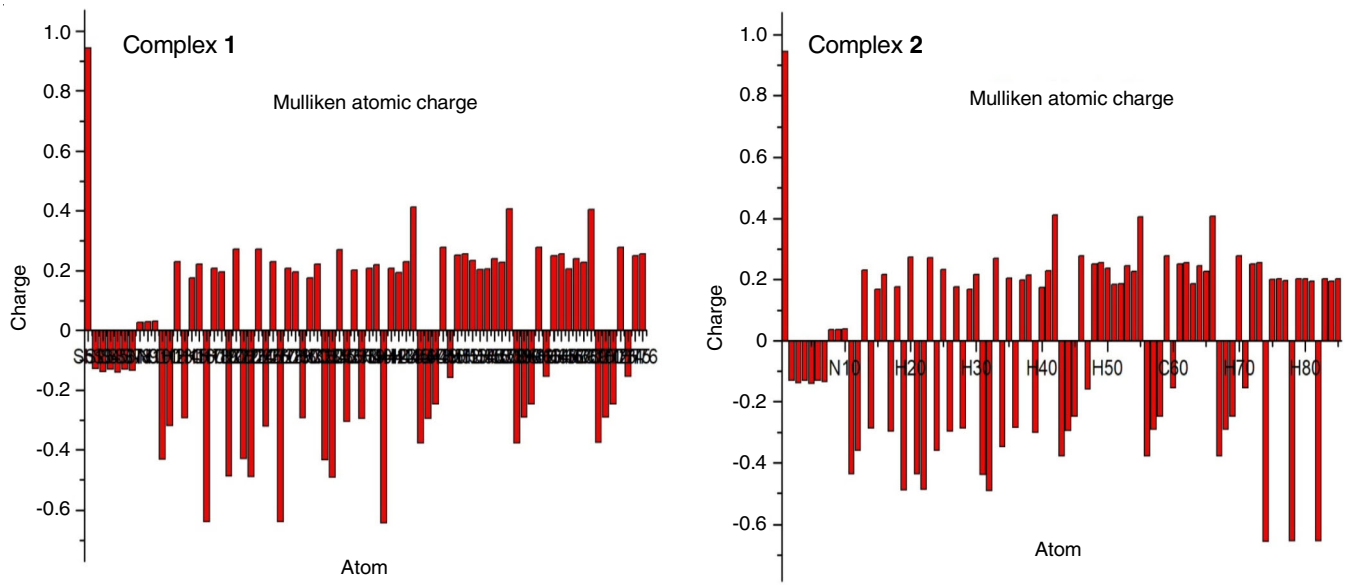

Fig. 6. Mulliken Atomic charge analysis of complexes **1** and **2**

Biological studies

Antimicrobial screening: Both antimony(III) complexes **1** and **2** were screened against two Gram-positive bacteria (*Klebsiella pneumoniae* and *Staphylococcus aureus*) and two Gram-negative bacteria (*Escherichia coli* and *Vibrio cholera*) and selected two fungi organism *Candida albicans* and *Aspergillus niger* by disc diffusion process at concentrations of 400 and 800 µg/disc. The activity of both complexes was evaluated by measuring the diameter of the inhibition region. The activity of the complexes were compared with ciprofloxacin (standard drug). Antimicrobial activities of the complexes are lower than those of the standard drug (ciprofloxacin) used. Table-6 indicates the increasing concentration of complexes; dosage level of from 400 to 800 µg/disc, the inhibitory effect was increased. All the tested antimony dithiocarbamate complexes exhibited lesser activity against *Escherichia coli*, *Staphylococcus aureus* and slightly higher activity against *Vibrio cholera*e and *Klebsiella pneumonia*e. The inhibitory activity of complex **1** was greater against *Vibrio cholera*e than those of complex **2**.

The antifungal studies exhibited that both complexes revealed moderate activity against tested selected fungal compared to the standard drug (ciprofloxacin). Complexes **1** and **2** demonstrated better activity towards *Aspergillus niger* and *Candida albicans*, respectively. It is found that the functionalization of N-bound of dithiocarbamate ligands in antimony(III) complexes does not affect antibacterial and antifungal activity of antimony(III) dithiocarbamate complexes.

Conclusion

Two new complexes (*tris*(*N*-furfuryl-*N*-propyldithiocarbamato-S,S′)antimony(III) (**1**) and *tris*(*N*-furfuryl-*N*-butyldithiocarbamato-S,S′)antimony(III) (**2**) have been characterized by CHN analysis, FT-IR, NMR (^{1}H & ^{13}C) spectra, antimicrobial and DFT studies. The FT-IR spectra of the complexes showed the contribution of thioureide ($\nu_{C\text{-}N}$) bonds to the structures. The ^{1}H and ^{13}C NMR spectra of the complexes clearly indicated that the instantaneous environment around the thioureide ($\nu_{C\text{-}N}$) nitrogen was mainly affected by compound formation. The thioureide ($\nu_{C\text{-}N}$) bond lengths were between 1.351 and 1.353 Å, clearly representing the flow of electron density from the nitrogen atom to the central metal ion. The bond angles of the ligands, appeared in the range 64.6-64.7 ° in complex **1**, organize the geometry around the antimony center. The chemical potential (µ) value is the lower for the complex **1** and slightly higher for the complex **2**. Electrophilicity value for the complex **1** is the slightly higher, whereas complex **2** is the lower. Electrophilicity is considered to be good if the chemical potential value is high and global hardness is low. The colour code of the complexes lies in the range of -9.161 e^{-3} to +9.161 e^{-3} and of -9.155 e^{-3} to +9.155 e^{-3} for complexes **1** and **2**, respectively. In the molecular electrostatic potential, the negative electrostatic potential regions are localized over the electronegative atoms and the positive electrostatic potential regions are localized over the hydrogen atoms of the complexes. The activity of the complexes were compared with ciprofloxacin. The inhibitory

TABLE-6
ANTIMICROBIAL ACTIVITY (DIAMETER OF INHIBITION ZONE) OF COMPLEXES **1** AND **2**

Complex	Disc content (µg)	Selected bacteria				Selected fungal	
		E. coli	*K. pneumoniae*	*S. aureus*	*V. cholera*	*A. niger*	*C. albicans*
1	400	08	11	09	12	11	14
	800	11	13	11	15	15	16
2	400	07	10	08	11	12	14
	800	11	13	12	14	14	15
Ciprofloxacin		34	36	27	35	28	38

activity of complex **1** was greater against *Vibrio cholera*e than those of complex **2**. The functionalization of N-bound organic moiety of dithiocarbamate ligands in antimony(III) complexes does not affect antibacterial and antifungal activity of antimony (III) dithiocarbamate complexes.

CONFLICT OF INTEREST

The authors declare that there is no conflict of interests regarding the publication of this article.

REFERENCES

1. S. Garje and V.K. Jain, *Coord. Chem. Rev.*, **236**, 35 (2003); https://doi.org/10.1016/S0010-8545(02)00159-5
2. S. Joshi, H.P.S. Chauhan and N. Carpenter, *J. Mol. Struct.*, **1128**, 221 (2017); https://doi.org/10.1016/j.molstruc.2016.08.063
3. S. Tamilvanan, G. Gurumoorthy, S. Thirumaran and S. Ciattini, *Polyhedron*, **123**, 111 (2017); https://doi.org/10.1016/j.poly.2016.10.026
4. J.O. Adeyemi and D.C. Onwudiwe, *Molecules*, **23**, 2571 (2018); https://doi.org/10.3390/molecules23102571
5. B.E. Causton, F.J.T. Burke and N.H.F. Wilson, *Dent. Mater.*, **9**, 209 (1993); https://doi.org/10.1016/0109-5641(93)90122-7
6. J.O. Adeyemi, D.C. Onwudiwe and E.C. Hosten, *J. Saudi Chem. Soc.*, **22**, 427 (2018); https://doi.org/10.1016/j.jscs.2017.08.004
7. E.J. Mensforth, M.R. Hill and S.R. Batten, *Inorg. Chim. Acta*, **403**, 9 (2013); https://doi.org/10.1016/j.ica.2013.02.019
8. M. Hrubaru, D.C. Onwudiwe, S. Shova, C. Draghici, L. Tarko and E.C. Hosten, *Inorg. Chim. Acta*, **471**, 257 (2018); https://doi.org/10.1016/j.ica.2017.11.010
9. F. Frézard, C. Demicheli, K.C. Kato, P.G. Reis and E.H. Lizarazo-Jaimes, *Rev. Inorg. Chem.*, **33**, 1 (2013); https://doi.org/10.1515/revic-2012-0006
10. V.R. Moreira, L.C.L. de Jesus, R.E.P. Soares, L.D.M. Silva, B.A.S. Pinto, M.N. Melo, A.M. de Andrade Paes and S.R.F. Pereira, *Antimicrob. Agents Chemother.*, **61**, e02360 (2017); https://doi.org/10.1128/AAC.02360-16
11. S.K. Hadjikakou, D.C. Antoniadis, N. Hadjiliadis, M. Kubicki, J. Binolis, S. Karkabounas and K. Charalabopoulos, *Inorg. Chim. Acta*, **358**, 2861 (2005); https://doi.org/10.1016/j.ica.2004.06.028
12. E.R.T. Tiekink, *Crit. Rev. Oncol. Hematol.*, **42**, 217 (2002); https://doi.org/10.1016/S1040-8428(01)00217-7
13. S. Yan, F. Li, K. Ding and H. Sun, *J. Biol. Inorg. Chem.*, **8**, 689 (2003); https://doi.org/10.1007/s00775-003-0468-1
14. J.O. Adeyemi and D.C. Onwudiwe, *Molecules*, **25**, 305 (2020); https://doi.org/10.3390/molecules25020305
15. S.K. Hadjikakou, I.I. Ozturk, C.N. Banti, N. Kourkoumelis and N. Hadjiliadis, *J. Inorg. Biochem.*, **153**, 293 (2015); https://doi.org/10.1016/j.jinorgbio.2015.06.006
16. D. Kafetzis, I. Velissariou, S. Stabouli, M. Mavrikou, D. Delis and G. Liapi, *Int. J. Antimicrob. Agents*, **25**, 26 (2005); https://doi.org/10.1016/j.ijantimicag.2004.09.011
17. S. Abdolmaleki, N. Yarmohammadi, H. Adibi, M. Ghadermazi, M. Ashengroph, H.A. Rudbari and G. Bruno, *Polyhedron*, **159**, 239 (2019); https://doi.org/10.1016/j.poly.2018.11.063
18. O. Urgut, I. Ozturk, C. Banti, N. Kourkoumelis, M. Manoli, A. Tasiopoulos and S. Hadjikakou, *Mater. Sci. Eng. C*, **58**, 396 (2016); https://doi.org/10.1016/j.msec.2015.08.030
19. I. Ozturk, S. Filimonova, S.K. Hadjikakou, N. Kourkoumelis, V. Dokorou, M.J. Manos, A.J. Tasiopoulos, M.M. Barsan, I.S. Butler, E.R. Milaeva, J. Balzarini and N. Hadjiliadis, *Inorg. Chem.*, **49**, 488 (2010); https://doi.org/10.1021/ic901442e
20. I.I. Ozturk, O.S. Urgut, C.N. Banti, N. Kourkoumelis, A.M. Owczarzak, M. Kubicki, K. Charalabopoulos and S.K. Hadjikakou, *Polyhedron*, **52**, 1403 (2013); https://doi.org/10.1016/j.poly.2012.04.038
21. I.I. Ozturk, C.N. Banti, N. Kourkoumelis, M.J. Manos, A.J. Tasiopoulos, A.M. Owczarzak, M. Kubicki and S.K. Hadjikakou, *Polyhedron*, **67**, 89 (2014); https://doi.org/10.1016/j.poly.2013.08.052
22. X. Hou, X. Li, H. Hemit and H.A. Aisa, *J. Coord. Chem.*, **67**, 461 (2014); https://doi.org/10.1080/00958972.2014.890717
23. Y. Liu and E.R.T. Tiekink, *CrystEngComm*, **7**, 20 (2005); https://doi.org/10.1039/b416493h
24. C. Kavounis, S. Kokkou, P. Rentzeperis and P. Karagiannidis, *Acta Crystallogr.*, **36**, 2954 (1980); https://doi.org/10.1107/S0567740880010606
25. P.J. Rani and S. Thirumaran, *Eur. J. Med. Chem.*, **62**, 139 (2013); https://doi.org/10.1016/j.ejmech.2012.12.047
26. R.X. Li, L. Zhou, P.P. Shi, X. Zheng, J.X. Gao, Q. Ye and D.W. Fu, *New J. Chem.*, **43**, 154 (2019); https://doi.org/10.1039/C8NJ03845G
27. H. Chermette, *J. Comput. Chem.*, **20**, 129 (1999); https://doi.org/10.1002/(SICI)1096-987X(19990115)20:1<129::AID-JCC13>3.0.CO;2-A
28. K. Ramirez-Balderrama, E. Orrantia-Borunda and N. Flores-Holguin, *J. Theor. Comput. Chem.*, **16**, 1750019 (2017); https://doi.org/10.1142/S0219633617500195
29. A. Zainuri, S. Arshad, N.C. Khalib and I.A. Razak, *Mol. Cry. Liq. Cryst.*, **650**, 87 (2017); https://doi.org/10.1080/15421406.2017.1328222
30. K. Chaturvedi, A. Kumar and A. Mishra, *Der Pharma Chem.*, **6**, 27 (2014).
31. L. Ronconi, L. Giovagnini, C. Marzano, F. Bettìo, R. Graziani, G. Pilloni and D. Fregona, *Inorg. Chem.*, **44**, 1867 (2005); https://doi.org/10.1021/ic048260v
32. F. Bonati and R. Ugo, *J. Organomet. Chem.*, **10**, 257 (1967); https://doi.org/10.1016/S0022-328X(00)93085-7
33. G. Hogarth, *Prog. Inorg. Chem.*, **53**, 71 (2005); https://doi.org/10.1002/0471725587.ch2
34. K. Wolinski, J.F. Hinton and P. Pulay, *J. Am. Chem. Soc.*, **112**, 8251 (1990); https://doi.org/10.1021/ja00179a005
35. A. Prasad, S.K. Kalainathan and S.P. Meenakshisundaram, *Optik (Stuttg.)*, **127**, 6134 (2016); https://doi.org/10.1016/j.ijleo.2016.04.060
36. T.A. Koopmans, *Physica*, **1**, 104 (1934); https://doi.org/10.1016/S0031-8914(34)90011-2
37. R.S. Mulliken, *J. Chem. Phys.*, **2**, 782 (1934); https://doi.org/10.1063/1.1749394
38. R.G. Parr, L. Szentpály and S. Liu, *J. Am. Chem. Soc.*, **121**, 1922 (1999); https://doi.org/10.1021/ja983494x
39. A. Kumar, R. Kumar, A. Gupta, P. Tandon and E.D. D'silva, *J. Mol. Struct.*, **1150**, 166 (2017); https://doi.org/10.1016/j.molstruc.2017.08.072
40. A.H. Anizaim, M.F. Zaini, M.A. Laruna, I.A. Razak and S. Arshad, *Acta Cryst.*, **E75**, 632 (2019); https://doi.org/10.1107/S2056989019004912